Linear response peculiarity of a two-dimensional Dirac electron gas at weak scattering

Andreas Sinner and Klaus Ziegler
Institut für Physik, Universität Augsburg, D-86135 Augsburg, Germany
(Received 17 September 2013; revised manuscript received 7 January 2014; published 29 January 2014)

The conductivity of an electron gas can be alternatively calculated either from the current-current or from the density-density correlation function. Here, we compare these two frequently used formulations of the Kubo formula for the two-dimensional Dirac electron gas by direct evaluations for several special cases. Assuming the presence of weak disorder, we investigate perturbatively both formulas at and away from the Dirac point. While to zeroth order in the disorder amplitude both formulations give identical results, with some very strong assumptions though, they show significant discrepancies already in first order. At half-filling, we evaluate all second-order diagrams. Virtually none of the topologically identical diagrams yield the same corrections for both formulations. We conclude that a direct comparison of conductivities of disordered system calculated in both formulas is not possible. The density-density correlation function is preferable since it can be linked to diffusion via the Einstein relation.

DOI: 10.1103/PhysRevB.89.024201 PACS number(s): 81.05.ue, 72.80.Vp, 72.10.Bg

I. INTRODUCTION

In this paper, we address the observation that different versions of the Kubo conductivity formula do not always lead to identical results. Without claiming the generality of this statement, we concentrate on the special case of a weakly disordered two-dimensional Dirac electron gas. On the one hand, there is a formulation in terms of the current-current correlation function, which represents the core object in the theory of weak localization in disordered metals in Refs. [1–8]. On the other hand, there is a formulation in terms of the density-density correlation function, which is preferably used in the theory of Anderson localization [9,10,12–16]. Although both formulations are obtained starting from the same initial point, the assumptions that need to be made in-between seem rather different. However, it is not the purpose of this paper to present a detailed discussion of these assumptions. This problem may go beyond the well-known fact that different limiting processes do not commute for the Kubo formula (cf. Ref. [17]). Rather, we want to point out the discrepancies at the level of practical calculations.

The conductivity at the Fermi energy μ, derived from linear response within the Kubo formalism, can be expressed either by the (properly normalized) current-current correlation function as

$$\bar{\sigma} = 2\,\mathrm{Tr}\sum_r j_n[\delta_\eta(H-\mu)]_{0r}\, j_n[\delta_\eta(H-\mu)]_{r0}, \tag{1}$$

where H denotes the Hamiltonian of the system under consideration, or by the density-density correlation function as

$$\bar{\sigma} = -\frac{\omega^2}{2}\mathrm{Tr}\sum_r r_n^2 G_{0r}\left(\frac{\omega}{2}-\mu+i\eta\right)G_{r0}\left(\frac{\omega}{2}-\mu-i\eta\right), \tag{2}$$

where the trace refers to spinor degrees of freedom and ω to the frequency of an external electric field. The scattering by static disorder has been included here by the phenomenological scattering rate η. It should be noticed that the prefactor ω^2 in the density-density form can be replaced for $\omega \ll \eta$ by $-4\eta^2$ since the transport is controlled by the scattering, represented by the scattering rate η, rather than by the frequency ω. This can be justified by the scaling relation [18]

$$\begin{aligned}\lim_{\epsilon\to 0}\mathrm{Tr}\sum_r r_n^2\left\langle G_{0r}\left(\frac{\omega}{2}+i\epsilon\right)G_{r0}\left(-\frac{\omega}{2}-i\epsilon\right)\right\rangle &= \frac{(\omega+2i\eta)^2}{\omega^2}\omega^2\mathrm{Tr}\sum_r r_n^2 G_{0,0r}\left(\frac{\omega}{2}+i\eta\right)\\ &\quad\times G_{0,r0}\left(-\frac{\omega}{2}-i\eta\right),\end{aligned} \tag{3}$$

where $G_{0,xy}$ (G_{xy}) denote the Green's function of the clean (disordered) system and $\langle\ldots\rangle$ is the averaging with respect to disorder. The prefactor $(1+2i\eta/\omega)^2$ appears as a consequence of the integration over the spontaneously broken chiral symmetry. Since ω breaks the chiral symmetry, the prefactor is finite for $\omega > 0$ and diverges only in the dc limit. From the point of view of spontaneous symmetry breaking, ω plays the role of a symmetry-breaking field, like the magnetic field in a ferromagnet, and η plays the role of the order parameter (magnetization). Replacing this prefactor by 1 gives us the self-consistent Born approximation. This implies that the self-consistent Born approximation is valid for high frequencies $\omega \gg \eta$ but not in the dc limit $\omega \ll \eta$.

In general, the density-density formulation (2) can be linked to diffusion via the Einstein relation [11,12] (cf. Sec. V). This is a more direct connection between diffusive quantum transport and correlations of the Green's functions than the linear response theory. Moreover, the connection between the two expressions in Eqs. (1) and (2) is due to the continuity equation (cf. Ref. [19]) $\omega\rho + \nabla\cdot\mathbf{j} = 0$, which can be used to replace the current operator by the density operator. In other words, we use the relation

$$j_n^2 = e^2 v_n^2 = (e r_n \omega)^2$$

in the current-current expression of the conductivity. This was discussed in more detail in Ref. [20]. However, the replacement must be taken with care due to certain limits. In particular, the dc limit $\omega \to 0$ can cause some problems, as we shall discuss in the following.

 ©2014 American Physical Society

The paper is organized as follows: We start with the analysis of the dc conductivity of the clean system in Sec. II. We show that both formulations lead to the same result which is in good agreement with the experimentally observed V-like shape of the conductivity as a function of the charge density. We discuss contributions from different band-scattering processes to the total conductivity. While contributions from intraband scattering dominate the contribution from interband scattering, the latter are not negligible even at large chemical potentials, in contrast to the naive expectation. We point out the subtlety of the reduced current-current formulation, i.e., hidden logarithmic divergences arising from each band-scattering process. In Sec. III, we proceed with the evaluation of perturbative diagrams of second order in the effective disorder strength at half-filling. We discuss the effect of different disorder types on the dc conductivity. In current-current language, we identify diagrams responsible for logarithmic divergences for a random chemical potential and a random mass. For the case of a random vector potential, we find in the current-current language finite second-order corrections, which is in clear contradiction to the established understanding of the physics of this particular disorder acquired from the density-density formula. Generally, we observe an entirely different behavior of topologically equivalent diagrams in both formulations, which originates from their different analytical structure. In Sec. IV, we then compare first-order perturbative corrections obtained from both formulas away from the Dirac point. We conclude the paper with a discussion and several appendices containing important technical details.

II. CONDUCTIVITY AT NONZERO CHEMICAL POTENTIAL

Our first goal is to evaluate the dc conductivity of the doped Dirac electron gas within the current-current formulation of Eq. (1). The δ functions in this expression are supposed to have a finite peak width η, i.e., the scattering rate, which plays the role of the finite ultraviolet cutoff parameter. For Dirac Hamiltonian $H = i\nabla\cdot\sigma$, the current operator j_n becomes

$$j_n = -i[H,r_n] = \sigma_n. \tag{4}$$

Using the relation between the δ function and resolvent of an operator $\mathcal{O}$,

$$\mathrm{Im}[\mathcal{O} \pm i\eta]^{-1} = \mp\delta_\eta(\mathcal{O}), \tag{5}$$

we may replace δ functions in Eq. (1) by

$$[\delta_\eta(H-\mu)]_{xy} = \frac{G_{xy}(-\mu - i\eta) - G_{xy}(-\mu + i\eta)}{2i}, \tag{6}$$

where $G_{xy}(-\mu \pm i\eta)$ denotes the Green's function of a particle propagating from the spatial point with coordinates x to the point with coordinates y forwardly (if $+i\eta$, i.e., retarded Green's function) or backwardly (if $-i\eta$, i.e., advanced Green's function) in time. This yields the following expression for the conductivity:

$$\bar{\sigma} = -\frac{1}{2}\mathrm{Tr}\sum_r \sigma_n[G_{0r}(-\mu - i\eta) - G_{0r}(-\mu + i\eta)] \times \sigma_n[G_{r0}(-\mu - i\eta) - G_{r0}(-\mu + i\eta)], \tag{7}$$

which has been used as the departure point for numerous investigations of transport, mainly in the context of the weak-localization approach [5–8]. In order to distinguish between the different terms we shall call combinations of advanced and retarded Green's functions

$$\sim \mathrm{Tr}\sum_r \sigma_n G_{0r}(-\mu - i\eta)\sigma_n G_{r0}(-\mu + i\eta) \tag{8a}$$

normal channel, and combinations with only advanced or only retarded Green's functions, e.g.,

$$\sim \mathrm{Tr}\sum_r \sigma_n G_{0r}(-\mu \pm i\eta)\sigma_n G_{r0}(-\mu \pm i\eta), \tag{8b}$$

anomalous channel. Moreover, we employ the Fourier representation to calculate the conductivity. The Green's functions then become

$$G_p(\pm i\eta - \mu) = \frac{\not{p} \mp i(\eta \pm i\mu)}{p^2 + (\eta \pm i\mu)^2}, \tag{9}$$

where we use the slashed notation $\not{p} = p\cdot\sigma = p_i\sigma_i$. Since $\sigma_n\not{p} = p_n\sigma_n\sigma_n - p_{l\neq n}\sigma_l\sigma_n = \not{p}^\dagger\sigma_n$, and $\not{p}^\dagger\not{p} \sim \cos(2\phi)$ vanishes under angular integration, all terms in the numerator containing p vanish altogether. After performing the trace with respect to the Dirac matrices, we obtain

$$\bar{\sigma} = \int_p \left[\frac{\eta - i\mu}{p^2 + (\eta - i\mu)^2} + \frac{\eta + i\mu}{p^2 + (\eta + i\mu)^2}\right]^2,$$

where $\int_p$ stands for the two-dimensional momentum integration $\int_{-\infty}^{+\infty} d^2p/(2\pi)^2$. For nonzero η and μ, the poles in this expression lie in the complex plane and we may perform integration along the real axis without going into the complex plane. While

$$\int_p \frac{(\eta \pm i\mu)^2}{[p^2 + (\eta \pm i\mu)^2]^2} = \frac{\bar{\sigma}_0}{4},$$

where $\bar{\sigma}_0 = 1/\pi$, another contribution gives

$$\int_p \frac{2(\eta - i\mu)(\eta + i\mu)}{[p^2 + (\eta - i\mu)^2][p^2 + (\eta + i\mu)^2]} = \frac{\bar{\sigma}_0}{2}\frac{\eta^2 + \mu^2}{\mu\eta}\mathrm{atan}\left(\frac{\mu}{\eta}\right).$$

Introducing $z = \mu/\eta$, we obtain for the conductivity

$$\bar{\sigma} = \frac{\bar{\sigma}_0}{2}\left(1 + \frac{1+z^2}{z}\mathrm{atan}(z)\right), \tag{10}$$

which is also obtained for the density-density formula in Appendix C. This conductivity is quite general for two-dimensional two-band systems with a spectral node [21]. At the Dirac point, i.e., for $\mu = 0$, this gives the universal minimal conductivity $\bar{\sigma}_0 = 1/\pi$ independently of the value of η.

Intuitively, one would expect that only states located in the vicinity of the Fermi energy $E_F = \mu$ contribute to the conductivity. In order to check this statement, we calculate explicitly contributions to the conductivity resulting from each band. Technical details are given in Appendix A. Denoting the upper ("conductance") band as the $+$ band and the lower ("valence") band as the $-$ band, the corresponding contributions from interband scattering are found

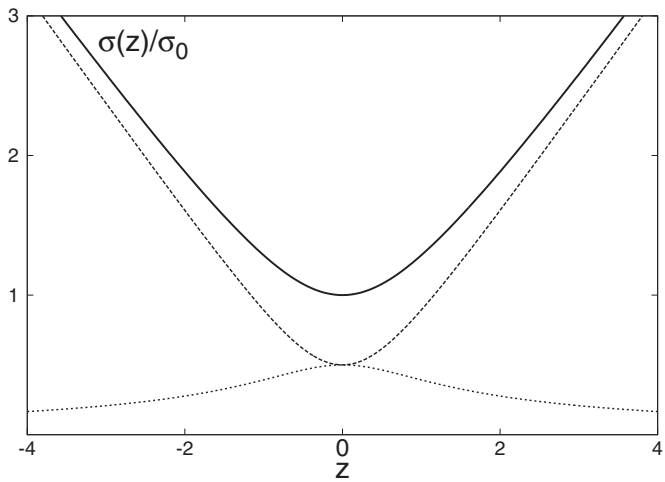

FIG. 1. Conductivity formula (10) (solid line) yields the well-known dependence on the chemical potential (i.e., the V shape with respect to charge density) reported in Ref. [22]. Dotted line shows the conductivity contribution from the interband scattering given in Eq. (11a), while the dashed line shows the contribution from the intraband scattering in Eq. (11b).

to be

$$\bar{\sigma}_{+-} = \bar{\sigma}_{-+} = \frac{\bar{\sigma}_0}{4z}\text{atan}(z). \tag{11a}$$

Thus, contributions from interband scattering *decrease* with increasing chemical potential μ or with decreasing scattering rate η. On the other hand, contributions from intraband scattering processes are given by

$$\bar{\sigma}_{++} = \bar{\sigma}_{--} = \frac{\bar{\sigma}_0}{4}[1 + z\,\text{atan}(z)], \tag{11b}$$

which *increase* with increasing chemical potential or decreasing scattering rate (cf. Fig. 1).

The reduced current-current formula, which takes only the normal channel of Eq. (8a) into account, is sometimes used for the conductivity calculations [5–8]. For this we consider as previously the projections onto the bands and obtain

$$\bar{\sigma}^N_{++} = \bar{\sigma}^N_{--} = \frac{\bar{\sigma}_0}{4}[\ell + z\,\text{atan}(z)], \quad \ell = \frac{1}{2}\ln\left(\frac{\Lambda^2}{\eta^2+\mu^2}\right) \tag{12a}$$

for the intraband and

$$\bar{\sigma}^N_{+-} = \bar{\sigma}^N_{-+} = \frac{\bar{\sigma}_0}{4}\left(-\ell + \frac{1}{z}\text{atan}(z)\right) \tag{12b}$$

for the interband contributions. Here, we have introduced the momentum cutoff Λ. While Eq. (8a) in total is finite, each projection acquires a logarithm, with different sign though, which may become very large at the Dirac point ($\mu \to 0$) due to the smallness of η. Equation (12a) is valid only for arguments of the logarithms of order unity, i.e., for the $\mu \sim \Lambda$ (~ 1 eV for graphene). This has led many authors to the conclusion that the perturbative calculation is only valid far away from the Dirac point (cf. [7]). In contrast to this statement, however, the inclusion of both bands in the conductivity leads to the cancellation of the logarithmic terms and we obtain a finite conductivity even at the Dirac node for arbitrarily weak scattering.

III. SECOND-ORDER PERTURBATION THEORY AT HALF-FILLING

While both expressions for the conductivity in Eqs. (1) and (2) give the same result in the self-consistent approximation, it would be interesting to see whether this also holds in perturbation theory with respect to disorder. The expressions have very different analytical structures and, therefore, they may behave differently once disorder is included. The envisaged task aims at the general understanding of this behavior and shall be pursued at the simplest possible level. Therefore, we study the conductivity perturbatively, assuming disorder to be weak. In our previous paper [23] we already studied the conductivity in the density-density formula and came to the conclusion that the perturbation series is free of logarithmic divergences, at least up to second order. Here, we perform an analogous investigation in the current-current formula. The relative simplicity of this formulation in comparison to the density-density language enables us to perform all calculations analytically in a fully controllable way. We consider in detail the case of the random scalar potential which plays the role of the spatially fluctuating chemical potential. We start with Eq. (7):

$$\langle\bar{\sigma}\rangle = -\frac{1}{2}\text{Tr}\sum_r \langle\sigma_n\,[G(-v-i\eta) - G(-v+i\eta)]_{0r} \times \sigma_n[G(-v-i\eta) - G(-v+i\eta)]_{r0}\rangle, \tag{13}$$

where $\langle\ldots\rangle$ denotes averaging with respect to a random chemical potential v with mean zero and with the Gaussian correlator

$$\langle v_r v_{r'}\rangle = g\delta(r-r'). \tag{14}$$

It is convenient to consider both normal and anomalous channels separately and sum over all contributions after the perturbative calculations are performed. Obviously, this is allowed by the linearity of the averaging process (a usual Gaussian integration). We emphasize that it is crucial to account for both normal and anomalous channels.

Taking the degeneracy into account, the conductivity in the normal channel reads as

$$\langle\bar{\sigma}_N\rangle = \text{Tr}\sum_r\langle\sigma_n G_{0r}(-v-i\eta)\sigma_n G_{r0}(-v+i\eta)\rangle, \tag{15}$$

while in the anomalous channel we have

$$\langle\bar{\sigma}_A\rangle = -\text{Tr}\sum_r\langle\sigma_n G_{0r}(-v-i\eta)\sigma_n G_{r0}(-v-i\eta)\rangle. \tag{16}$$

The topology of the diagrams is the same in both channels. Figure 2 shows the zeroth-order diagram (see Table I),

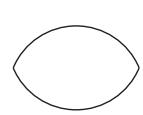

FIG. 2. Zeroth-order diagram.

TABLE I. Contributions to universal conductivity in both channels from the zeroth-order diagram (Fig. 2) in units of $\bar{\sigma}_0$.

Diagram	Normal channel	Anomalous channel	Both channels	Ref. [23]
◯ × 1	1/2	1/2	1	1

contributing to the universal dc conductivity. There are 3 diagrams in each channel in first order, as depicted in Fig. 3 and 15 diagrams in second order shown in Fig. 4.

The detailed evaluation of all first- and second-order diagrams in the current-current formula is represented in Appendix B. The evaluation of first-order diagrams in the density-density formula is shown in Appendix C. The results of those calculations are summarized in Tables II and III. The difference between the two formulas could not be more striking. Virtually none of the diagrams have the same value in both formulas. Both normal and anomalous channels in the current-current formula do not contribute to the conductivity on the same footing but seem to compete at every order. As one of the results of this competition, there is no conductivity correction to order g at all, while in the density-density formula such a correction certainly exists. A similar situation is also observed to the order g^2. In analogy to the density-density formula, we see here that diagrams with and without intersection of impurity lines, i.e., ◯, ◯, both ◯, and all four ◯ on one hand and ◯, both ◯, and both ◯ on the other, build up disjoint subsets. Logarithmic divergences of diagrams without disorder line intersections cancel exactly in both formulas. This is even the case in both channels in the current-current formula, in an entirely different way though. On the contrary, diagrams with intersecting disorder lines behave differently not only in both formulas, but also in both channels in the current-current formula. In density-density formula, the structure is too complicated to be evaluated analytically. Their evaluation with MATHEMATICA in Ref. [23] led us to the conclusion that each of them vanish separately by angular integration. In contrast, the analytical structure of these diagrams in the current-current language makes an analytical evaluation possible. It turns out that each of these diagrams diverges only logarithmically, in contrast to diagrams without intersections, which diverge as a squared logarithm. The amplitudes of the topologically equivalent diagrams are the same in both channels but the sign is different such that these logarithms cancel each other in the anomalous channel but sum themselves up in the normal channel to a global logarithmic singularity. Taking all the contributions to order g^2, the conductivity in current-current formula reads as

$$\frac{\langle\bar{\sigma}\rangle}{\bar{\sigma}_0} \approx 1 + \frac{\alpha^2}{4} + 2\alpha^2(\ell - c_v), \tag{17}$$

where $\alpha = g/2\pi$, $c_v \sim 1.5518$, and $\ell = \ln\Lambda/\eta$. The logarithmic divergence in Eq. (17) looks very similar to the usual weak-antilocalization term [3], but it is not since the latter is due to the massless cooperon mode which can not be seen in any finite order of the perturbative expansion. This divergence resembles more what was called the *ultraviolet logarithmic corrections* in Ref. [24].

In analogy to the case of random chemical potential, we are able to calculate perturbative corrections also for other disorder types. Following, we briefly summarize results of these calculations.

Random mass. The case of the random mass is of particular interest since it governs a metal-insulator transition. This disorder type has been intensively studied for the couple of decades, both analytically [18,25,26] and more recently numerically [27,28]. This potential couples to the Pauli matrix σ_3 and anticommutes with the Hamiltonian of the clean system. This leads to some differences in the calculation. Again, we see significant discrepancies with our previous work [23] in both orders. All diagrams which vanish for the random chemical potential do vanish for the random mass as well, in particular diagrams ◯, ◯, and ◯. Contributions from diagrams ◯ and ◯ average to zero after summing over both channels. As in the case of the random scalar potential, we also observe ◯ + 2◯ = 0 in both channels independently. Therefore, the leading-order correction is again of the order g^2. Diagram ◯ is finite, while diagrams ◯ and ◯ diverge logarithmically. The total conductivity to second order reads as

$$\frac{\langle\bar{\sigma}\rangle}{\bar{\sigma}_0} \approx 1 + \frac{\alpha^2}{4} + 2\alpha^2(\ell + c_m) \tag{18}$$

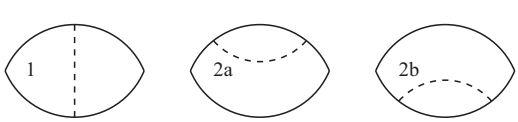

FIG. 3. First-order diagrams.

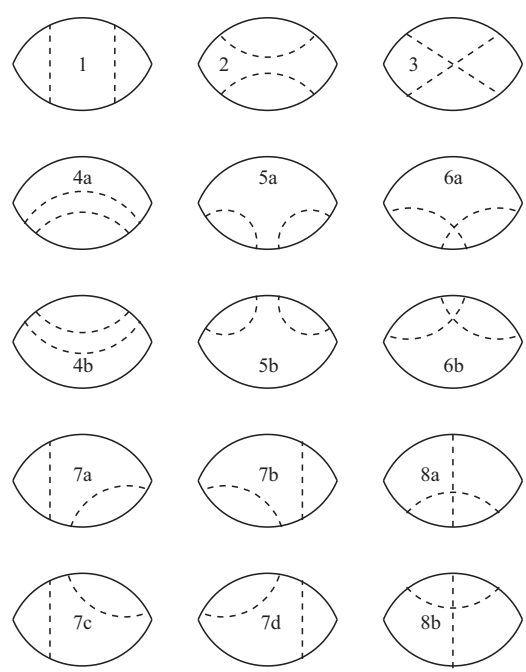

FIG. 4. Second-order diagrams.

TABLE II. Conductivity corrections from the first-order diagrams (Fig. 3) in units of the universal conductivity $\bar{\sigma}_0$, $\alpha = g/2\pi$, $\ell = \ln \Lambda/\eta$.

Diagram	Normal channel	Anomalous channel	Both channels	Ref. [23]
× 1	$\alpha/4$	$-\alpha/4$	0	$\alpha[1+2\ell]$
× 2	0	0	0	$-2\alpha\ell$
Total	$\alpha/4$	$-\alpha/4$	0	α

with the constant $c_m \approx 1.1052$. Interestingly, the logarithm was not observed numerically in Ref. [27].

Random vector potential. This disorder type is usually associated with the surface corrugations which arise due to thermal instability of two-dimensional crystals. It was shown in the density-density formalism [29,30] that this disorder type does not change the universal value of the conductivity, so we might expect this to be true also in the current-current formula. Because of the vector nature of this potential $v \to a_i\sigma_i$, $i = 1,2$, the Gaussian correlator is changed to

$$\langle a_i(x)a_j(x')\rangle = g\delta_{ij}\delta(x-x'). \tag{19}$$

All diagrams which give zero contributions for the other disorder types vanish for the case of the random vector potential too. Also, the relation + 2 = 0 holds in both channels. The major difference to other disorder types consists in the behavior of the diagrams with intersecting disorder lines: they do not develop any logarithmic divergences. Instead, they obey a beautiful relation + 2 + 2 = 0 in each channel with the relative weights of each diagram, respectively, $1, \frac{1}{2}, -1$. However, diagram yields a finite contribution which is not compensated by any other terms. In contrast to the exact result of Ref. [29], we find that the conductivity acquires finite corrections as

$$\frac{\langle\bar{\sigma}\rangle}{\bar{\sigma}_0} \approx 1 + \alpha^2, \tag{20}$$

which clearly deviates from the previous results.

IV. LEADING-ORDER PERTURBATION THEORY AT NONZERO CHEMICAL POTENTIAL

Our next task is to extend the perturbative analysis to a nonzero chemical potential. In this section, we compute the leading-order perturbative corrections in disorder strength to Eq. (10). We start with Eq. (7), average over disorder, and reorder terms due to each channel:

$$\langle\bar{\sigma}\rangle = \mathrm{Tr}\int_p \langle\sigma_n G_p(-\mu - i\eta)\sigma_n G_p(-\mu + i\eta)\rangle \tag{21a}$$

$$-\frac{1}{2}\mathrm{Tr}\sum_{s=\pm}\int_p \langle\sigma_n G_p(-\mu + is\eta)\sigma_n G_p(-\mu + is\eta)\rangle. \tag{21b}$$

Expanding to leading order in g we obtain from Eq. (21a)

$$g\mathrm{Tr}\int_p G_p(-\mu - i\eta)\sigma_n G_p(-\mu + i\eta) \times \int_q G_q(-\mu + i\eta)\sigma_n G_q(-\mu - i\eta) + g\mathrm{Tr}\sum_{s=\pm}\int_q G_q(-\mu + is\eta) \tag{22a}$$

$$\int_p G_p(-\mu + is\eta)\sigma_n G_p(-\mu - is\eta)\sigma_n G_p(-\mu + is\eta), \tag{22b}$$

and from Eq. (21b)

$$-\frac{g}{2}\mathrm{Tr}\sum_{s=\pm}\int_p G_p(-\mu + is\eta)\sigma_n G_p(-\mu + is\eta) \times \int_q G_q(-\mu + is\eta)\sigma_n G_q(-\mu + is\eta) - g\mathrm{Tr}\sum_{s=\pm}\int_q G_q(-\mu + is\eta) \tag{22c}$$

$$\int_p G_p(-\mu + is\eta)\sigma_n G_p(-\mu + is\eta)\sigma_n G_p(-\mu + is\eta). \tag{22d}$$

TABLE III. Conductivity corrections from the second-order diagrams (Fig. 4) in units of the universal conductivity $\bar{\sigma}_0$, $\alpha = g/2\pi$, $\ell = \ln \Lambda/\eta$. The constant c is calculated in Eq. (B9b) with the numerical value ∼3.1036.

Diagram	Normal channel	Anomalous channel	Both channels	Ref. [23]
× 1	$\alpha^2/8$	$\alpha^2/8$	$\alpha^2/4$	$\alpha^2[1+4\ell+6\ell^2]/2$
× 1	$\alpha^2\ell^2/6$	$\alpha^2\ell^2/6$	$\alpha^2\ell^2/3$	$5\alpha^2\ell^2/3$
× 2	$-\alpha^2\ell^2/6$	$-\alpha^2\ell^2/6$	$-\alpha^2\ell^2/3$	$4\alpha^2\ell^2/3$
× 4	0	0	0	$-4\alpha^2\ell[1+\ell]$
× 2	0	0	0	$2\alpha^2\ell[1-\ell]$
× 1	$-\alpha^2[c-2\ell]/4$	$-\alpha^2[c-2\ell]/4$	$-\alpha^2[c-2\ell]/2$	0
× 2	$-\alpha^2[c-2\ell]/2$	$\alpha^2[c-2\ell]/2$	0	0
× 2	$-\alpha^2[c-2\ell]/4$	$-\alpha^2[c-2\ell]/4$	$-\alpha^2[c-2\ell]/2$	0
Total	$\alpha^2(1-8c+16\ell)/8$	$\alpha^2/8$	$\alpha^2(1-4c+8\ell)/4$	$\alpha^2/2$

Diagrammatically, Eqs. (22a) and (22c) correspond to and Eqs. (22b) and (22d) to both diagrams which become different (complex conjugated of each other) at nonzero chemical potential. Equations (22c) and (22d) represent contributions to the conductivity from the anomalous channel and are much easier to evaluate. Because they contain either only retarded or only advanced Green's functions, the evaluation does not differ much from the undoped case. Equation (22d) gives zero and

$$\text{Eq. (22c)} = -\frac{\bar{\sigma}_0}{4}\alpha. \tag{23}$$

In contrast, Eqs. (22a) and (22b) require more effort. Concerning Eq. (22b), we obtain after performing the q integral the trace and angular integral in the p part

$$\text{Eq. (22b)} = 2g\sum_{s=\pm}\frac{\eta^2+\mu^2}{(4\pi)^2}\ln\left(\frac{\Lambda^2}{\eta^2+\mu^2}e^{-2is\,\mathrm{atan}\frac{\mu}{\eta}}\right) \times\int_0^\infty dt\,\frac{t-(\eta+is\mu)^2}{[t+(\eta+is\mu)^2]^2[t+(\eta-is\mu)^2]},$$

where $t = p^2$. After performing the partial fraction decomposition under the t integral

$$\frac{t-A^2}{[t+A^2]^2[t+B^2]} = \frac{\alpha}{t+A^2} - \frac{\alpha}{t+B^2} + \frac{\beta}{[t+A^2]^2}$$

with

$$\alpha = \frac{A^2+B^2}{(A^2-B^2)^2},\quad \beta = \frac{2A^2}{A^2-B^2},$$

it can be easily evaluated. We obtain

$$\text{Eq. (22b)} = \frac{4g}{(2\pi)^2}\sum_{s=\pm}\frac{\eta^2+\mu^2}{4\mu\eta}\left[-2\,\mathrm{atan}\frac{\mu}{\eta} - is\,\ln\frac{\Lambda^2}{\eta^2+\mu^2}\right] \times\left[1-\frac{\eta^2-\mu^2}{\eta\mu}\mathrm{atan}\frac{\mu}{\eta}\right],$$

such that the imaginary parts cancel each other upon summation over s and the final result does not depend on the cutoff Λ. Eventually, we arrive at the following total contribution from all -like diagrams:

$$\sum_{\text{all}} = -\frac{\bar{\sigma}_0\alpha}{2}\frac{1+z^2}{z}\mathrm{atan}(z)\left(1-\frac{1-z^2}{z}\mathrm{atan}(z)\right). \tag{24}$$

The remaining contribution (22a) corresponds to the normal channel correction from the diagram. Since both q and p integrals give equal contributions to the final result, we obtain

$$\text{Eq. (22a)} = \frac{\bar{\sigma}_0\alpha}{4}\left(\int_0^\infty dt\,\frac{\eta^2+\mu^2}{[t+(\eta+i\mu)^2][t+(\eta-i\mu)^2]}\right)^2 = \frac{\bar{\sigma}_0\alpha}{4}\left(\frac{1+z^2}{z}\mathrm{atan}(z)\right)^2.$$

Then, the total contribution from all -like diagrams reads as

$$\sum_{\text{all}} = \frac{\bar{\sigma}_0\alpha}{4}\left[\left(\frac{1+z^2}{z}\mathrm{atan}(z)\right)^2 - 1\right]. \tag{25}$$

Equations (24) and (25) together give the total first-order correction in g for Eq. (10). It vanishes for $z \to 0$ in accord to our calculations of Sec. III. In the other limit $z \to \infty$ it becomes negative

$$\frac{\langle\bar{\sigma}\rangle - \bar{\sigma}}{\bar{\sigma}_0} \sim -\alpha\frac{\pi^2 z^2}{16}, \tag{26}$$

where $\bar{\sigma}$ is given by Eq. (10). For comparison, in Appendix C we have evaluated the same diagrams in the density-density formalism with the result given in Eq. (C19). While for small z both expressions behave very differently, the large-z behavior is similar. In both cases, it goes $\sim -z^2$ with the only difference of factor 2 in the weight. For small z, both expressions are plotted in Fig. 4.

V. DISCUSSION

In this paper, we have carried out a comparative analysis of two frequently used particular formulations of the Kubo conductivity formula for the case of a weakly disordered two-dimensional Dirac electron gas in the dc limit: the current-current and density-density formulas. Even a superficial glimpse at these formulas, as they are given by Eqs. (1) and (2), suffices to recognize that they are structurally different from each other. Mainly, the difference is due to the fact that the current operator is up to a constant a nondiagonal Pauli matrix. Therefore, the intermixing of the bands occurs in the current-current formula, whereas in the density-density formula this is not the case. Fortunately, however, for the clean and even for the disordered system in the self-consistent Born approximation both formulas provide us with the very same expression at and away from the Dirac point, as it is given in Eq. (10) and shown in Fig. 1. Generally, we conclude that the dc transport behavior of the two-dimensional Dirac electron gas becomes more conventional as we go deeper in the conduction band because interband scattering becomes less important. The difference of both formulations, however, becomes evident if one computes corrections to the conductivity in terms of disorder strength. To leading order they are shown in Fig. 5 as

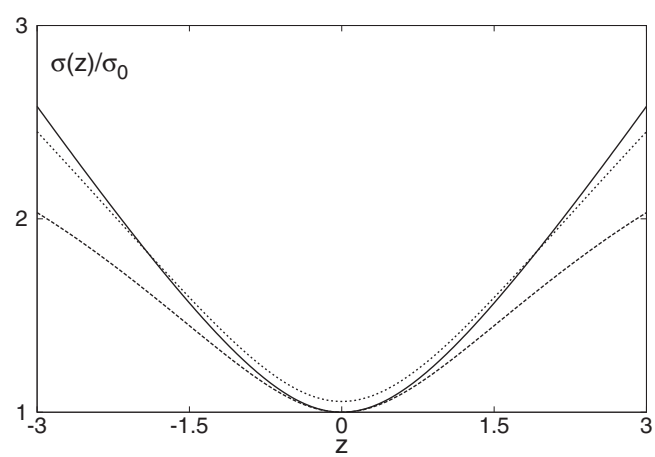

FIG. 5. Corrected dc conductivity in comparison to the conductivity in Born-approximation equation (10) (solid line). Dashed curve shows the result from the current-current formula, dotted line that from the density-density formula plotted for $\alpha \approx 0.1$.

functions of the chemical potential. The correction obtained for the density-density formula reveals a weaker dependence on the chemical potential since it barely deviates from the Dirac point value up to $z = \pm 1$. In contrast, the correction obtained from the current-current formula reveals a substantial deviation from the Dirac point value already at $z \sim \pm 0.5$.

The properties of both conductivities do not deviate dramatically in our calculation. A qualitative comparison with the experimentally observed V shape of the conductivity as a function of the charge density [22] can be matched by both expressions, after fitting the scattering rate η properly (cf. Fig. 5). Thus, a comparison with experimental data can not decide over the validity of the two Kubo formulas, as long as we do not have accurate measurements of the scattering rate. As we go to higher orders of corrections, we may find stronger deviations. This is indicated by the results of the weak-localization approach, which includes partial summations of infinitely many perturbation terms. The current-current correlation function provides in this case a logarithmically increasing conductivity [6]

$$\sigma = \frac{e^2}{h}\left[\frac{8}{g} + \frac{4}{\pi}\ln\left(\frac{\mu}{\mu_\phi}\right)\right], \tag{27}$$

where μ_ϕ is a phenomenological parameter due to inelastic scattering which vanishes for a vanishing temperature. In contrast to this expression, the density-density correlation function gives us Eq. (10) again [31]. These results clearly indicate that only the density-density correlation gives the V-shape conductivity.

A more direct support for the density-density formula comes from the Einstein relation: the physics of dc transport in the presence of weak scattering should be governed by the diffusion of quasiparticles. This relation has been used in many studies of disorder scattering to express the conductivity through the density-density correlation for one-band metals [11,12] and for two-band metals [21,32]. For this purpose, we introduce the probability for a quasiparticle to move from site $\mathbf{r}'$ to site $\mathbf{r}$ during the time t with probability $P_{\mathbf{r}\mathbf{r}'}(t) = |\langle\mathbf{r}|\exp(-iHt)|\mathbf{r}'\rangle|^2$, where H is the hopping Hamiltonian. Then, the mean-square displacement with respect to $\mathbf{r}' = 0$ describes diffusion if the following equation is satisfied:

$$\langle r_k^2\rangle = \sum_{\mathbf{r}} r_k^2 P_{\mathbf{r},0}(t) = Dt. \tag{28}$$

Using the Green's function we obtain for large distances $|\mathbf{r} - \mathbf{r}'|$ and $\epsilon \sim 0$

$$\int_0^\infty P_{\mathbf{r}\mathbf{r}'}(t)e^{-\epsilon t}dt \sim \int_{E_0}^{E_F}\langle G_{\mathbf{r}\mathbf{r}'}(E+i\epsilon)G_{\mathbf{r}'\mathbf{r}}(E-i\epsilon)\rangle dE, \tag{29}$$

where E_0 is the lower band edge. Then, we get from Eq. (29) for the diffusion coefficient at energy E

$$D(E) \sim \lim_{\epsilon\to 0}\epsilon^2\sum_{\mathbf{r}} r_k^2\langle G_{\mathbf{r}0}(E+i\epsilon)G_{0\mathbf{r}}(E-i\epsilon)\rangle_d \tag{30}$$

with $D = \int D(E)\rho(E)dE$ in Eq. (28) and with the density of states ρ. For transport at low temperatures, we need the diffusion coefficient only at the Fermi energy E_F. This expression agrees with the density-density formula (2) since the dc conductivity can be calculated from $D(E)$ via the Einstein relation $\sigma \propto \rho(E_F)D(E_F)$.

In conclusion, we have found that perturbative corrections for both conductivity formulas differ substantially from each other in every order and even for every type of diagram. This is a problem of the dc limit since the equivalence of the formulas for $\omega \gg \eta$ is easy to show [20]. Our findings question the comparability of results acquired by different calculational methods since in some cases the density-density formula, in other cases the current-current formula, have been used. From our comparison with diffusion we would conclude that the density-density formula is preferable. A challenge would be to reformulate the weak-localization approach in terms of the density-density formula and to compare it with the nonlinear sigma-model approach, which is based on the density-density formula. A first attempt in this direction can be found in Ref. [31].

ACKNOWLEDGMENT

We acknowledge useful discussions with E. Hankiewicz and R. Raimondi.

APPENDIX A: CONTRIBUTIONS TO CONDUCTIVITY FROM DIFFERENT BAND-SCATTERING PROCESSES

In order to estimate the relative importance of interband versus intraband scattering, it is convenient to go into the representation in which Green's functions are diagonal. The unitary transformation diagonalizing them reads as

$$U_p = \frac{1}{\sqrt{2}}\begin{pmatrix} \frac{p_1 - ip_2}{p} & \frac{p_1 - ip_2}{p} \\ 1 & -1 \end{pmatrix}, \tag{A1}$$

with $p = \sqrt{p_1^2 + p_2^2}$. In the diagonal representation, Green's functions become $\hat{G}_p = U_p^* G_p U_p$, i.e.,

$$\hat{G}_p(\pm i\eta - \mu) = \frac{p\sigma_3 \mp i(\eta \pm i\mu)}{p^2 + (\eta \pm i\mu)^2}. \tag{A2}$$

The conductivity in diagonal representation reads as

$$\bar{\sigma} = -\frac{1}{2}\mathrm{Tr}\int_p [\hat{G}_p(-i\eta - \mu) - \hat{G}_p(i\eta - \mu)] \times \hat{\sigma}_n\sigma_0[\hat{G}_p(-i\eta - \mu) - \hat{G}_p(i\eta - \mu)]\hat{\sigma}_n\sigma_0, \tag{A3}$$

where current operators in diagonal representation are

$$\hat{\sigma}_n = U_p^*\sigma_n U_p. \tag{A4}$$

The contributions from each band-scattering process can be found by expanding the unity operator σ_0 in the basis of orthogonal projectors on each subband:

$$\sigma_0 = \mathcal{P}_+ + \mathcal{P}_- = \frac{\sigma_0 + \sigma_3}{2} + \frac{\sigma_0 - \sigma_3}{2}. \tag{A5}$$

The projectors act on the Green's functions as follows:

$$\mathcal{P}_\pm\frac{p\sigma_3 \mp i(\eta \pm i\mu)}{p^2 + (\eta \pm i\mu)^2} = \mathcal{P}_\pm\frac{\pm p \mp i(\eta \pm i\mu)}{p^2 + (\eta \pm i\mu)^2}, \tag{A6}$$

and we obtain the following expressions for an intraband contribution:

$$\bar{\sigma}_{++} = -\frac{1}{2}\int_p \mathrm{Tr}\{\hat{\sigma}_n\mathcal{P}_+\hat{\sigma}_n\mathcal{P}_+\}\left[\frac{p+i(\eta+i\mu)}{p^2+(\eta+i\mu)^2} - \frac{p-i(\eta-i\mu)}{p^2+(\eta-i\mu)^2}\right]^2,$$

and correspondingly for $\bar{\sigma}_{--}$, as well as for an interband contribution

$$\bar{\sigma}_{+-} = -\frac{1}{2}\int_p \mathrm{Tr}\,\{\hat{\sigma}_n\mathcal{P}_+\hat{\sigma}_n\mathcal{P}_-\}\left[\frac{p+i(\eta+i\mu)}{p^2+(\eta+i\mu)^2} - \frac{p-i(\eta-i\mu)}{p^2+(\eta-i\mu)^2}\right]\left[\frac{-p+i(\eta+i\mu)}{p^2+(\eta+i\mu)^2} - \frac{-p-i(\eta-i\mu)}{p^2+(\eta-i\mu)^2}\right],$$

and correspondingly for $\bar{\sigma}_{-+}$. Calculating partial traces yields

$$\mathrm{Tr}\,\{\hat{\sigma}_n\mathcal{P}_+\hat{\sigma}_n\mathcal{P}_+\} = \frac{p_n^2}{p^2} \quad \text{and} \quad \mathrm{Tr}\,\{\hat{\sigma}_n\mathcal{P}_+\hat{\sigma}_n\mathcal{P}_-\} = \frac{p_{l\neq n}^2}{p^2},$$

i.e., a factor $\frac{1}{2}$ due to angular integration. After carrying out multiplications and partial fraction decomposition in the remaining integrals we arrive at

$$\bar{\sigma}_{++} = \frac{1}{4}\int_p\left[\frac{\eta}{i\mu}\left(\frac{1}{p^2+(\eta-i\mu)^2} - \frac{1}{p^2+(\eta+i\mu)^2}\right) + \frac{2(\eta-i\mu)^2}{[p^2+(\eta-i\mu)^2]^2} + \frac{2(\eta+i\mu)^2}{[p^2+(\eta+i\mu)^2]^2}\right]$$

and

$$\bar{\sigma}_{+-} = \frac{\eta}{4i\mu}\int_p\left(\frac{1}{p^2+(\eta-i\mu)^2} - \frac{1}{p^2+(\eta+i\mu)^2}\right),$$

and analogously for $\bar{\sigma}_{--}$ and $\bar{\sigma}_{-+}$. A straightforward integration finally yields Eqs. (11a) and (11b).

APPENDIX B: EVALUATION OF DIAGRAMS IN CURRENT-CURRENT FORMULA

1. First-order diagrams

We start with the diagram . For the normal channel it reads in real space representation as

$$= g\mathrm{Tr}\sum_{r,x}\sigma_n G_{r0}(-i\eta)\sigma_n G_{0x}(i\eta)G_{xx}(i\eta)G_{xr}(i\eta),$$

and correspondingly for the anomalous channel

$$= -g\mathrm{Tr}\sum_{r,x}\sigma_n G_{r0}(-i\eta)\sigma_n \times G_{0x}(-i\eta)G_{xx}(-i\eta)G_{xr}(-i\eta).$$

Transforming into the Fourier space yields (here for both channels)

$$= \pm g\mathrm{Tr}\int_q G_q(\pm i\eta)\int_p G_p(\pm i\eta)\sigma_n G_p(-i\eta)\sigma_n G_p(\pm i\eta),$$

which enables one to perform integrations over momenta q and p separately. While the former diverges logarithmically as $\ln(\Lambda/\eta)$ with the upper cutoff Λ, the latter is zero:

$$\int_p \frac{[\not{p}\mp i\eta][\not{p}^\dagger+i\eta][\not{p}\mp i\eta]}{[p^2+\eta^2]^3} \sim \int_0^\infty dt\,\frac{t-1}{[t+1]^3} = 0,$$

where $t = p^2/\eta^2$ since terms containing odd powers of p_i and $\not{p}\not{p}^\dagger$ vanish after the angular integration. For large Λ, this expression goes to zero $\sim \Lambda^{-2}$ and therefore faster than $\ln\Lambda^{-1}$.

Next, we consider diagram . For both channels it reads in real space representation as

$$= \pm g\mathrm{Tr}\sum_{r,x}\sigma_n G_{0x}(-i\eta)G_{xr}(-i\eta)\sigma_n G_{rx}(\pm i\eta)G_{x0}(\pm i\eta).$$

Changing into the Fourier representation gives

$$= \pm g\mathrm{Tr}\int_p G_p(\pm i\eta)\sigma_n G_p(-i\eta)\int_q G_q(-i\eta)\sigma_n G_q(\pm i\eta).$$

Again, both momentum integrals can be carried out separately, e.g.,

$$\int_q G_q(-i\eta)\sigma_n G_q(\pm i\eta) = \sigma_n\int_q \frac{[\not{q}^\dagger+i\eta][\not{q}\mp i\eta]}{[q^2+\eta^2]^2} = \pm\frac{\sigma_n}{4\pi}.$$

The total correction from these diagrams is

$$= \pm\frac{2g}{(4\pi)^2} = \pm\frac{\bar{\sigma}_0\alpha}{4},$$

where $\alpha = g/2\pi$, and their sum is zero.

2. Second-order diagrams

The evaluation of the second-order diagrams without intersecting disorder lines is largely analogous to the just considered first-order case. In particular, one can easily see in analogy to the diagram that diagrams and vanish as well. On the contrary, the evaluation of the diagrams with intersecting disorder lines is technically much more demanding. We start with the easier case of the diagram . In real-space representation, it reads as (for another diagram of the class analogously)

$$= \pm g^2\mathrm{Tr}\sum_{r,x,y}\sigma_n G_{r0}(\mp i\eta)\sigma_n G_{0x}(i\eta) \times G_{xy}(i\eta)G_{yx}(i\eta)G_{xy}(i\eta)G_{yr}(i\eta). \tag{B1}$$

Transforming into the Fourier space and shifting momenta appropriately, we arrive at

$$= \pm g^2\mathrm{Tr}\int_k\int_q G_{q+k}(i\eta)G_q(i\eta) \times \int_p G_p(i\eta)\sigma_n G_p(\mp i\eta)\sigma_n G_p(i\eta)G_{p+k}(i\eta).$$

We start with the integral over q:

$$\mathcal{A} = \int_q G_{q+k}(i\eta)G_q(i\eta) = \int_q \frac{[\not{q} + \not{k} - i\eta][\not{q} - i\eta]}{[(k+q)^2+\eta^2][q^2+\eta^2]}.$$

It is convenient to evaluate this integral using Feynman parametrization

$$\frac{1}{AB} = \int_0^1 dx \frac{1}{[(1-x)A + xB]^2}. \tag{B2}$$

Then, taking $A = q^2 + \eta^2$ and symmetrizing the denominator by a momentum shift $q_i \to q_i - xk_i$ we get

$$\mathcal{A} = \int_0^1 dx \int_q \frac{[\not{q} + (1-x)\not{k} - i\eta][\not{q} - x\not{k} - i\eta]}{[q^2+\eta^2+x(1-x)k^2]^2}.$$

The denominator represents an even function in momenta q and therefore all terms containing odd powers of q in the numerator can be dropped. We get

$$\mathcal{A} = \int_0^1 dx \int_q \left\{ \frac{q^2 - \eta^2 - (1-x)k^2}{[q^2+\eta^2+x(1-x)k^2]^2} - \frac{i\eta(1-2x)\not{k}}{[q^2+\eta^2+x(1-x)k^2]^2} \right\}.$$

The second term in this expression does not survive under the x integration. Indeed, since

$$1 - 2x = \frac{d}{dx}[x(1-x)], \tag{B3}$$

we can substitute $x(1-x) = y$. It is possible since x enters the remaining part only via $x(1-x)$. Then, the y integration runs over an empty set since $x(1-x) = 0$ for both $x = 0$ and 1. Integration in the first term is simple. We obtain with $\ell = \ln\Lambda/\eta$ and $t = k^2/\eta^2$

$$\mathcal{A} = \frac{1}{2\pi}[\ell - 1] - \frac{1}{4\pi}\int_0^1 dx\ \ln[1 + x(1-x)t] = \frac{1}{2\pi}\left[\ell - \sqrt{\frac{4+t}{t}}\operatorname{atanh}\sqrt{\frac{t}{4+t}}\right]. \tag{B4}$$

For the evaluation of the x integral, it is convenient to decompose the argument of the logarithm as

$$1 + x(1-x)t = (i\sqrt{t}[x - x_+])(i\sqrt{t}[x - x_-]), \tag{B5}$$

where the poles are given by

$$x_\pm = \frac{1}{2}\left(1 \pm \sqrt{1 + \frac{4}{t}}\right), \tag{B6}$$

with the properties

$$1 - x_\pm = x_\mp,\ \ x_+ + x_- = 1,\ \text{and}\ \ x_+x_- = -\frac{1}{t}. \tag{B7}$$

Then, the x integration can be performed via the usual log-integration formula $\int dx\ \ln x = x\ \ln x - x$. Importantly, Eq. (B4) is even under $k \to -k$ (since $t = k^2/\eta^2$). This is significant for the remaining integral over the momentum p since we can also neglect terms containing odd powers of k_i in the numerator after symmetrizing the denominator with respect to p. In order to perform such symmetrization, we employ a generalization of the Feynman parametrization:

$$\frac{1}{A^{1+n}B} = \frac{(-1)^n}{n!}\frac{\partial^n}{\partial\alpha^n}\bigg|_{\alpha=0}\frac{1}{[\alpha + A]B} = \frac{(-1)^n}{n!}\frac{\partial^n}{\partial\alpha^n}\bigg|_{\alpha=0}\int_0^1 dx\frac{1}{[(1-x)(\alpha+A)+xB]^2} = \int_0^1 dx\frac{(n+1)(1-x)^n}{[(1-x)A+xB]^{2+n}}. \tag{B8}$$

The validity of the formula (B8) can be verified by a straightforward integration over x. Thus, for the p integral we have

$$\mathcal{B} = \int_p G_p(i\eta)\sigma_n G_p(\mp i\eta)\sigma_n G_p(i\eta)G_{p+k}(i\eta) = 3\mathrm{Tr}\int_0^1 dx(1-x)^2 \times \int_p \frac{[\not{p} - i\eta][\not{p}^\dagger \pm i\eta][\not{p} - i\eta][\not{p} + \not{k} - i\eta]}{[(1-x)(p^2+\eta^2) + x(\eta^2 + (p+k)^2)]^4}.$$

Shifting momentum $p_i \to p_i - xk_i$ symmetrizes the denominator. Dropping odd powers of p_i, k_i, as well as $\not{p}\not{p}^\dagger$ and $\not{k}\not{k}^\dagger$, we get

$$[\not{p} - x\not{k} - i\eta][\not{p}^\dagger - x\not{k}^\dagger \pm i\eta][\not{p} - x\not{k} - i\eta] \times [\not{p} + (1-x)\not{k} - i\eta] \to \pm\eta^2[3p^2 - \eta^2 - x(2-3x)k^2],$$

where we use the identities of the type $\not{p}\not{k}\not{p}^\dagger = \not{k}^\dagger p^2$. The integrals are easily performed giving

$$\mathcal{B} = \pm 3\eta^2\mathrm{Tr}\int_0^1 dx(1-x)^2\int_p \frac{3p^2 - \eta^2 - x(2-3x)k^2}{[p^2+\eta^2+x(1-x)k^2]^4} = \pm\frac{1}{4\pi\eta^2}\int_0^1 dx\frac{(1-x)^2[1 - x(1-3x)t]}{[1+x(1-x)t]^3} = \mp\frac{1}{4\pi\eta^2}\frac{4\sqrt{t(4+t)} - 8(2+t)\operatorname{atanh}\sqrt{\frac{t}{4+t}}}{[t(4+t)]^{3/2}},$$

where again $t = k^2/\eta^2$. In order to calculate the integral over x we decomposed the denominator in accord with Eq. (B5) and performed a partial fraction decomposition. The remaining integrals over k (i.e., t) are innocent and can be performed numerically (for instance using MATHEMATICA):

$$\mp\int_0^\infty dt\frac{4\sqrt{[t(4+t)]} - 8(2+t)\operatorname{atanh}\sqrt{\frac{t}{4+t}}}{[t(4+t)]^{3/2}} = \pm 2, \tag{B9a}$$

$$\pm\int_0^\infty dt\sqrt{\frac{4+t}{t}}\operatorname{atanh}\sqrt{\frac{t}{4+t}} \times \frac{4\sqrt{[t(4+t)]} - 8(2+t)\operatorname{atanh}\sqrt{\frac{t}{4+t}}}{[t(4+t)]^{3/2}} \approx \mp 3.1036. \tag{B9b}$$

This yields the same conductivity correction for both channels

$$= \bar{\sigma}_0\frac{\alpha^2}{8}(2\ell - c), \tag{B10}$$

where $c \approx 3.1036$ and $\alpha = g/2\pi$.
Next, we consider diagram . In real-space representation it reads as

$$= \pm g^2 \mathrm{Tr} \sum_{r,x,y} \sigma_n G_{ry}(\mp i\eta) G_{y0}(\mp i\eta)\sigma_n \times G_{0x}(i\eta) G_{xy}(i\eta) G_{yx}(i\eta) G_{xr}(i\eta).$$

Fourier transforming and shifting the momenta yields

$$= \pm g^2 \mathrm{Tr} \int_p \int_q G_q(\mp i\eta)\sigma_n G_q(i\eta) G_{q+p}(i\eta) \times \int_k G_{k+p}(i\eta) G_k(i\eta)\sigma_n G_k(\mp i\eta).$$

We evaluate the q integral in details: We get rid of the current operators and use Feynman parametrization (B8):

$$\mathcal{C} = \int_q \frac{[\not{q}^\dagger \pm i\eta][\not{q} - i\eta][\not{q} + \not{p} - i\eta]}{[q^2+\eta^2]^2[(q+p)^2+\eta^2]} = 2\int_0^1 dx(1-x) \int_q \frac{[\not{q}^\dagger \pm i\eta][\not{q} - i\eta][\not{q} + \not{p} - i\eta]}{[(1-x)q^2 + x(q+p)^2 + \eta^2]^3}.$$

Symmetrization of the denominator is achieved by shifting $q_i \to q_i - xp_i$ such that odd powers of q_i in the numerator as well as terms containing $\not{q}^\dagger \not{q}$ can be dropped. With some algebra in-between, the numerator becomes

$$[\not{q}^\dagger - x\not{p}^\dagger \pm i\eta][\not{q} - x\not{p} - i\eta][\not{q} + (1-x)\not{p} - i\eta] = (\pm i\eta - 2x\not{p}^\dagger)[q^2 + \eta^2 + x(1-x)p^2] - (\pm 2i\eta - 3x\not{p}^\dagger)[\eta^2 + x(1-x)p^2] \pm (1-2x)\eta^2 \not{p}.$$

Terms containing $x(1-2x)$ are not shown here since they do not survive under the x integration. The integration over q can now be carried out and we get

$$\mathcal{C} = -\frac{1}{4\pi}\int_0^1 dx \left[\frac{x(1-x)\not{p}^\dagger}{\eta^2 + x(1-x)p^2} \mp \frac{(1-x)(1-2x)\eta^2\not{p}}{[\eta^2 + x(1-x)p^2]^2}\right].$$

The k integral gives the same result. We multiply both expressions, perform the trace, carry out angular integral, and introduce $t = p^2/\eta^2$. The result is

$$= \pm \frac{2g^2}{(4\pi)^3}\int_0^\infty \frac{dt}{t}\left(\int_0^1 dx \frac{x(1-x)t}{1+x(1-x)t}\right)^2 \pm \frac{2g^2}{(4\pi)^3}\int_0^\infty \frac{dt}{t}\left(\int_0^1 dx \frac{(1-x)(1-2x)t}{[1+x(1-x)t]^2}\right)^2.$$

The second x integral can be reduced to the first by an integration by parts:

$$\int_0^1 dx \frac{(1-x)(1-2x)t}{[1+x(1-x)t]^2} = -\int_0^1 dx(1-x)\frac{\partial}{\partial x}\frac{1}{1+x(1-x)t} = 1 - \int_0^1 dx \frac{1}{1+x(1-x)t} = \int_0^1 dx \frac{x(1-x)t}{1+x(1-x)t}.$$

The x integral can be easily calculated, which yields for the diagram

$$= \pm \frac{4g^2}{(4\pi)^3}\int_0^\infty \frac{dt}{t}\left(1 - \frac{4}{t}\sqrt{\frac{t}{4+t}}\,\mathrm{atanh}\sqrt{\frac{t}{4+t}}\right)^2. \tag{B11}$$

The expression in the brackets behaves well for all t. For $t \to 0$ it goes to $t/6$ and therefore the integral is innocent at the lower integration boundary. For $t \to \infty$ it approaches unity and the integral diverges logarithmically,

$$\int^{e^{2\ell}} \frac{dt}{t} \sim 2\ell, \tag{B12}$$

since $t \propto k^2$. Numerical evaluation gives

$$\int_0^{e^{2\ell}} \frac{dt}{t}\left(1 - \frac{4}{t}\sqrt{\frac{t}{4+t}}\,\mathrm{atanh}\sqrt{\frac{t}{4+t}}\right)^2 = 2\ell - c,$$

where $c \approx 3.1036$. The conductivity contribution is

$$= \pm\bar{\sigma}_0 \frac{\alpha^2}{4}(2\ell - c), \tag{B13}$$

and gives zero by summing over both channels.
The last diagram reads in Fourier representation as

$$= \pm g^2 \mathrm{Tr} \int_q \int_p G_p(\mp i\eta)\sigma_n G_p(i\eta) G_{p+q}(i\eta) \times \int_k G_k(i\eta)\sigma_n G_k(\mp i\eta) G_{k-q}(\mp i\eta),$$

which resembles strongly the just considered diagram . The evaluation goes analogously with some minor changes. For instance, while evaluating integral over k, the momenta should be shifted as $k_i \to k_i + xq_i$. The result has the same numerical value with the same sign in both channels:

$$= \bar{\sigma}_0 \frac{\alpha^2}{4}(2\ell - c). \tag{B14}$$

APPENDIX C: DENSITY-DENSITY FORMULA

1. Band contributions

Making use of the scaling relation (3), we write the Kubo formula for dc conductivity in the density-density formula with an artificial replacement of the frequency by some small but finite quantity η usually associated with the inverse scattering time:

$$\begin{aligned}\bar{\sigma} &= 2\eta^2 \mathrm{Tr} \sum_r r_n^2 G_{0r}(-\mu + i\eta) G_{r0}(-\mu - i\eta)\\ &= -2\eta^2 \left.\frac{\partial^2}{\partial q_n^2}\right|_{q=0} \mathrm{Tr} \int_p G_p(-\mu + i\eta) G_{p+q}(-\mu - i\eta)\\ &= 2\eta^2 \mathrm{Tr} \int_p G_p(-\mu + i\eta)\sigma_n G_p(-\mu + i\eta)\\ &\quad \times G_p(-\mu - i\eta)\sigma_n G_p(-\mu - i\eta),\end{aligned} \tag{C1}$$

where in the last line we performed a partial integration and used then the usual differentiation formula for matrices

$\partial_x A^{-1} = -A^{-1}\partial_x A A^{-1}$. Next, we go into the diagonal representation and project out. The $\bar{\sigma}_{++}$ and $\bar{\sigma}_{+-}$ contributions then read as

$$\bar{\sigma}_{++} = 2\eta^2 \mathrm{Tr}\int_p \hat{G}_p(-\mu+i\eta)\hat{\sigma}_n\mathcal{P}_+\hat{G}_p(-\mu+i\eta) \times \hat{G}_p(-\mu-i\eta)\hat{\sigma}_n\mathcal{P}_+\hat{G}_p(-\mu-i\eta), \tag{C2}$$

$$\bar{\sigma}_{+-} = 2\eta^2 \mathrm{Tr}\int_p \hat{G}_p(-\mu+i\eta)\hat{\sigma}_n\mathcal{P}_+\hat{G}_p(-\mu+i\eta) \times \hat{G}_p(-\mu-i\eta)\hat{\sigma}_n\mathcal{P}_-\hat{G}_p(-\mu-i\eta). \tag{C3}$$

We perform the trace and angular integration:

$$\bar{\sigma}_{++} = \frac{\eta^2}{2\pi}\int_0^\infty dp\, p\frac{[p+i(\eta-i\mu)]^2[p-i(\eta+i\mu)]^2}{[p^2+(\eta-i\mu)^2]^2[p^2+(\eta+i\mu)^2]^2} = \frac{\bar{\sigma}_0}{4}[1+z\mathrm{atan}(z)], \tag{C4}$$

$$\bar{\sigma}_{+-} = \frac{\eta^2}{2\pi}\int_0^\infty dp\, p\frac{1}{[p^2+(\eta-i\mu)^2][p^2+(\eta+i\mu)^2]} = \frac{\bar{\sigma}_0}{4z}\mathrm{atan}(z). \tag{C5}$$

Counting all contributions together gives Eq. (10).

2. First-order perturbation theory at half-filling

Consider disorder-averaged conductivity for the case of scalar disorder

$$\bar{\sigma} = -2\eta^2 \left.\frac{\partial^2}{\partial q_n^2}\right|_{q=0} \mathrm{Tr}\int_p \langle G_p(i\eta)G_{p+q}(-i\eta)\rangle, \tag{C6}$$

where $\langle\ldots\rangle$ denotes averaging with respect to disorder. Performing first perturbative expansion and then derivatives with respect to q_n we arrive at

$$\bar{\sigma} = -4g\eta^2\mathrm{Tr}\int_k G_k(i\eta)\int_p G_p(i\eta)G_p(-i\eta)\sigma_n G_p(-i\eta)\sigma_n G_p(-i\eta)G_p(i\eta) \tag{C7a}$$

$$-4g\eta^2\mathrm{Tr}\int_k G_k(-i\eta)\int_p G_p(-i\eta)G_p(i\eta)\sigma_n G_p(i\eta)\sigma_n G_p(i\eta)G_p(-i\eta) \tag{C7b}$$

$$-4g\eta^2\mathrm{Tr}\int_k G_k(i\eta)G_k(-i\eta)\int_p G_p(-i\eta)\sigma_n G_p(-i\eta)\sigma_n G_p(-i\eta)G_p(i\eta) \tag{C7c}$$

$$-4g\eta^2\mathrm{Tr}\int_k G_k(-i\eta)G_k(i\eta)\int_p G_p(i\eta)G_p(-i\eta)\sigma_n G_p(-i\eta)\sigma_n G_p(-i\eta) \tag{C7d}$$

$$-4g\eta^2\mathrm{Tr}\int_k G_k(-i\eta)\sigma_n G_k(-i\eta)G_k(i\eta)\int_p G_p(i\eta)G_p(-i\eta)\sigma_n G_p(-i\eta). \tag{C7e}$$

Equations (C7a) and (C7b) correspond to both diagrams, while Eqs. (C7c), (C7d), and (C7d) together represent the contribution from the diagram . Bearing in mind that

$$G_p(i\eta)G_p(-i\eta) = \frac{1}{p^2+\eta^2} \quad\text{and}\quad \int_p G_p(\pm i\eta) = \mp\frac{\ell}{2\pi},$$

we immediately obtain for each contribution

$$\text{Eq. (C7a)} = \text{Eq. (C7b)} = -\bar{\sigma}_0\alpha\ell, \tag{C8}$$

$$\text{Eq. (C7c)} = \text{Eq. (C7d)} = \bar{\sigma}_0\alpha\ell, \tag{C9}$$

$$\text{Eq. (C7e)} = \bar{\sigma}_0\alpha. \tag{C10}$$

Evidently, the sum of all contributions is free of logarithms but finite in contrast to the same order perturbative correction from the current-current formula, where it is zero.

3. First-order perturbation theory at nonzero chemical potential

We start with diagrams and perform first the derivatives:

$$\sum_{\text{all}} = -2g\eta^2 \left.\frac{\partial^2}{\partial q_n^2}\right|_{q=0} \mathrm{Tr}\sum_{s=\pm}\int_k G_k(-\mu+is\eta)\int_p G_p(-\mu+is\eta)G_{p+q}(-\mu-is\eta)G_p(-\mu+is\eta)$$
$$= -4g\eta^2\mathrm{Tr}\sum_{s=\pm}\int_k G_k(-\mu+is\eta)\int_p G_p(-\mu+is\eta)G_p(-\mu-is\eta)\sigma_n G_p(-\mu-is\eta)\sigma_n G_p(-\mu-is\eta)G_p(-\mu+is\eta).$$

Using the notation $A = \eta - is\mu$ and $B = \eta + is\mu$, we obtain for the k integral

$$\int_k G_k(-\mu + is\eta) = -is\frac{A}{4\pi}\ln\frac{\Lambda^2}{A^2}, \tag{C11}$$

and for the p integral

$$\begin{aligned}&\mathrm{Tr}\int_p G_p(-\mu+is\eta)G_p(-\mu-is\eta)\sigma_n G_p(-\mu-is\eta)\sigma_n G_p(-\mu-is\eta)G_p(-\mu+is\eta)\\ &= is\frac{B}{2\pi}\int_0^\infty dt\frac{t^2+t(4AB-A^2-B^2)+A^2B^2}{[t+A^2]^2[t+B^2]^3}.\end{aligned}$$

Performing the partial fraction decomposition with the coefficients

$$\alpha_1 = \frac{2AB-3A^2-B^2}{(A-B)^2(A+B)^4},\quad \beta_2 = -\frac{A-B}{(A+B)^3},$$
$$\alpha_2 = -\frac{2A^2}{(A-B)(A+B)^3},\quad \beta_3 = \frac{2B^2}{(A+B)^2},$$

we obtain for the conductivity correction from the -diagram class

$$\sum_{\text{all}} \bigcirc = -\bar{\sigma}_0\alpha\eta^2\sum_{s=\pm}AB\,\ln\frac{\Lambda^2}{A^2}\left(\alpha_1\ln\frac{B^2}{A^2}+\frac{\alpha_2}{A^2}+\frac{\beta_2}{B^2}+\frac{1}{2}\frac{\beta_3}{B^4}\right).$$

Since $A + B = 2\eta$, the factor η^2 in front drops out. Using

$$\ln\frac{\Lambda^2}{A^2} = \ln\frac{\Lambda^2}{\mu^2+\eta^2} + 2is\,\mathrm{atan}\left(\frac{\mu}{\eta}\right)\quad\text{and}\quad \ln\frac{B^2}{A^2} = 4is\,\mathrm{atan}\left(\frac{\mu}{\eta}\right) \tag{C12}$$

eventually leads us to the following expression:

$$\sum_{\text{all}} \bigcirc = -\frac{\bar{\sigma}_0\alpha}{2}\left[\ell\left(1+\frac{1+z^2}{z}\mathrm{atan}(z)\right)+\frac{1+3z^2}{2z}\mathrm{atan}(z)-\frac{1-2z^2-3z^4}{2z^2}\mathrm{atan}^2(z)\right] \tag{C13}$$

with $2\ell = \ln\frac{\Lambda^2}{\eta^2+\mu^2}$. As $z \to 0$, we reproduce Eq. (C8).

Next, we evaluate the diagram . Upon taking the derivatives with respect to q_n we have

$$\begin{aligned}\bigcirc &= -2g\eta^2\left.\frac{\partial^2}{\partial q_n^2}\right|_{q=0}\mathrm{Tr}\int_p G_p(-\mu+i\eta)G_{p+q}(-\mu-i\eta)\int_k G_{k+q}(-\mu-i\eta)G_k(-\mu+i\eta)\\ &= -4g\eta^2\mathrm{Tr}\int_p G_p(-\mu+i\eta)G_p(-\mu-i\eta)\sigma_n G_p(-\mu-i\eta)\sigma_n G_p(-\mu-i\eta)\int_k G_k(-\mu-i\eta)G_k(-\mu+i\eta) &\text{(C14a)}\\ &\quad -4g\eta^2\mathrm{Tr}\int_p G_p(-\mu+i\eta)G_p(-\mu-i\eta)\int_k G_k(-\mu-i\eta)\sigma_n G_k(-\mu-i\eta)\sigma_n G_k(-\mu-i\eta)G_k(-\mu+i\eta) &\text{(C14b)}\\ &\quad -4g\eta^2\mathrm{Tr}\int_p G_p(-\mu+i\eta)G_p(-\mu-i\eta)\sigma_n G_p(-\mu-i\eta)\int_k G_k(-\mu-i\eta)\sigma_n G_k(-\mu-i\eta)G_k(-\mu+i\eta). &\text{(C14c)}\end{aligned}$$

Obviously, Eqs. (C14a)–(C14c) reduce to Eqs. (C7c)–(C7e) as $\mu \to 0$. Equations (C14a) and (C14b) give identical contributions. Both integrals can be carried out separately. After performing the trace we get

$$-16g\eta^2\int\frac{d^2k}{(2\pi)^2}\frac{k^2+\mu^2+\eta^2}{[k^2+(\eta+i\mu)^2][k^2+(\eta-i\mu)^2]}\int\frac{d^2p}{(2\pi)^2}\frac{i(\eta+i\mu)\{i(\eta+i\mu)[p^2+\mu^2+\eta^2]-2\mu p^2\}}{[p^2+(\eta-i\mu)^2][p^2+(\eta+i\mu)^2]^3}. \tag{C15}$$

Introducing $A = \eta - i\mu$ and $B = \eta + i\mu$, we get by the partial fraction decomposition

$$\bar{\sigma}_0\alpha\eta^2 B\int_0^\infty dx\left(\frac{\alpha}{x+A^2}+\frac{\beta}{x+B^2}\right)\int_0^\infty dy\left[a_1\left(\frac{1}{y+A^2}-\frac{1}{y+B^2}\right)+\frac{b_2}{(y+B^2)^2}+\frac{b_3}{(y+B^2)^3}\right] \tag{C16}$$

with

$$\alpha = \frac{A}{A+B},\quad \beta = \frac{B}{A+B},\quad a_1 = -\frac{A}{(A-B)(A+B)^3},\quad b_2 = -\frac{A}{(A+B)^2},\quad\text{and}\quad b_3 = \frac{2B^2}{A+B}.$$

The integration over x yields

$$2[\ell + z\,\mathrm{atan}(z)],$$

while the y integration gives after multiplication with B

$$\frac{1}{4\eta^2}\left(1 + \frac{1+z^2}{z}\mathrm{atan}(z)\right).$$

Piecing all terms together gives for the contribution

$$\text{Eq. (C14a)} + \text{Eq. (C14b)} = \frac{\bar{\sigma}_0\alpha}{2}[\ell + z\,\mathrm{atan}(z)]\left(1 + \frac{1+z^2}{z}\mathrm{atan}(z)\right). \tag{C17}$$

Evidently, terms which contain ℓ are precisely the same as those appearing in in Eq. (C13) but with the opposite sign. Therefore, the ℓ-dependent terms will have gone after summing them. Equation (C14c) does not develop any logarithms. This contribution can be written after performing the trace as

$$\frac{1}{2}\bar{\sigma}_0\alpha\eta^2\left(A\int_0^\infty dx\frac{AB+x}{[x+A^2][x+B^2]^2}\right)^2 = \frac{1}{8}\bar{\sigma}_0\alpha\left(1 + \frac{1+z^2}{z}\mathrm{atan}(z)\right)^2. \tag{C18}$$

Therefore, the total first-order conductivity correction in density-density formula reads as

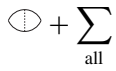 $+ \sum_{\text{all}}$ $= \frac{\bar{\sigma}_0\alpha}{8}\left(1 + \frac{3+2z^2-z^4}{z^2}\mathrm{atan}^2(z)\right),$ (C19)

with the both limits $\bar{\sigma}_0\alpha/2$ as $z \to 0$ and $-\bar{\sigma}\alpha\pi^2 z^2/32$ as $z \to \infty$.

[1] L. G. Gor'kov, A. I. Larkin, and D. E. Khmel'nitskii, Pis'ma Zh. Eksp. Teor. Fiz. **30**, 248 (1979) [JETP Lett. **30**, 228 (1979)].
[2] B. L. Altshuler, D. E. Khmel'nitskii, A. I. Larkin, and P. A. Lee, Phys. Rev. B **22**, 5142 (1980); B. L. Altshuler and B. D. Simons, in *Mesoscopic Quantum Physics*, edited by E. Akkermans *et al.* (North-Holland Publishing, Amsterdam 1995).
[3] S. Hikami, A. Larkin, and Y. Nagaoka, Prog. Theor. Phys. **63**, 707 (1980).
[4] B. L. Altshuler, A. G. Aronov, A. I. Larkin, and D. E. Khmel'nitskii, Zh. Eksp. Teor. Fiz. **81**, 768 (1981) [Sov. Phys. JETP **54**, 411 (1981)].
[5] T. Ando, Y. Zheng, and H. Suzuura, J. Phys. Soc. Jpn. **71**, 1318 (2002).
[6] E. McCann and V. I. Falko, Phys. Rev. Lett. **96**, 086805 (2006); E. McCann, K. Kechedzhi, V. I. Falko, H. Suzuura, T. Ando, and B. L. Altshuler, *ibid.* **97**, 146805 (2006).
[7] H. Suzuura and T. Ando, Phys. Rev. Lett. **89**, 266603 (2002).
[8] D. V. Khveshchenko, Phys. Rev. Lett. **97**, 036802 (2006).
[9] F. Wegner, Z. Physik B **35**, 207 (1979).
[10] L. Schäfer and F. Wegner, Z. Physik B **38**, 113 (1980).
[11] F. J. Wegner, Phys. Rev. B **19**, 783 (1979).
[12] A. J. McKane and M. Stone, Ann. Phys. (NY) **131**, 36 (1981).
[13] S. Hikami, Phys. Rev. B **24**, 2671 (1981).
[14] K. B. Efetov, Adv. Phys. **32**, 53 (1983); *Supersymmetry in Disorder and Chaos* (Cambridge University Press, New York, 1997).
[15] E. Fradkin, Phys. Rev. **33**, 3257 (1986); **33**, 3263 (1986).
[16] F. Wegner, Nucl. Phys. B **316**, 663 (1989).
[17] K. Ziegler, Phys. Rev. B **75**, 233407 (2007).
[18] K. Ziegler, Phys. Rev. Lett. **102**, 126802 (2009); Phys. Rev. B **79**, 195424 (2009).
[19] R. Kubo, M. Troda, and N. Hashitsume, *Statistical Physics*, Vol. II (Springer, Berlin, 1992).
[20] K. Ziegler, Phys. Rev. B **78**, 125401 (2008).
[21] K. Ziegler, Eur. Phys. J. B **86**, 391 (2013).
[22] K. S. Novoselov, A. K. Geim, S. V. Morozov, D. Jiang, M. I. Katsnelson, I. V. Grigorieva, S. V. Dubonos, and A. A. Firsov, Nature (London) **438**, 197 (2005).
[23] A. Sinner and K. Ziegler, Phys. Rev. B **84**, 233401 (2011).
[24] I. L. Aleiner and K. B. Efetov, Phys. Rev. Lett. **97**, 236801 (2006).
[25] K. Ziegler, Phys. Rev. B **55**, 10661 (1997); K. Ziegler and G. Jug, Z. Phys. B **104**, 5 (1997); K. Ziegler, Phys. Rev. Lett. **80**, 3113 (1998).
[26] M. Bocquet, D. Serban, and M. R. Zirnbauer, Nucl. Phys. B **578**, 628 (2000).
[27] J. H. Bardarson, M. V. Medvedyeva, J. Tworzydło, A. R. Akhmerov, and C. W. J. Beenakker, Phys. Rev. B **81**, 121414(R) (2010).
[28] M. V. Medvedyeva, J. Tworzydło, and C. W. J. Beenakker, Phys. Rev. B **81**, 214203 (2010).
[29] A. W. W. Ludwig, M. P. A. Fisher, R. Shankar, and G. Grinstein, Phys. Rev. B **50**, 7526 (1994).
[30] M. J. Bhaseen, I. I. Kogan, O. A. Soloviev, N. Taniguchi, and A. Tsvelik, Nucl. Phys. B **580**, 688 (2000); M. J. Bhaseen, J.-S. Caux, I. I. Kogan, and A. M. Tsvelik, *ibid.* **618**, 465 (2001).
[31] K. Ziegler and A. Sinner, arXiv:1311.3441.
[32] K. Ziegler, J. Phys. A: Math. Theor. **45**, 335001 (2012).